Materials Horizons

ROYAL SOCIETY OF CHEMISTRY

COMMUNICATION

View Article Online
View Journal | View Issue

Cite this: *Mater. Horiz.*, 2024, 11, 5352

Received 25th June 2024,
Accepted 1st August 2024

DOI: 10.1039/d4mh00812j

rsc.li/materials-horizons

Inspired by lubricin: a tailored cartilage-armor with durable lubricity and autophagy-activated antioxidation for targeted therapy of osteoarthritis†

Peng Yu,[a] Xu Peng,[b] Hui Sun,[a] Qiangwei Xin,[a] Han Kang,[c] Peng Wang,[a] Yao Zhao,[a] Xinyuan Xu,[a] Guangwu Zhou,[d] Jing Xie *[a] and Jianshu Li *[ae]

Osteoarthritis (OA), which disables articular cartilage, affects millions of people. The self-healing capacity is inhibited by internal oxidative stress and external lubrication deficiency and enzymatic degradation. To overcome these challenges, a tailored cartilage-armor is designed to ameliorate the inflamed cartilage, which is implemented by a novel collagen type II (Col II)-binding peptide conjugated zwitterionic polymer (PSB-*b*-PColBP, PSP). By mimicking natural lubricin, PSP specifically targets the cartilage surface and forms an *in situ* hydration armor. This engineered cartilage-armor can prevent enzymatic cartilage degradation (nearly 100% resistance to catabolic enzymes) and provide durable lubrication properties (COF $<$ 0.013 for 500 cycles). An autophagy-activation process, absent in previous biomimetic lubricants, enhances the enzymatic activity of the tailored cartilage-armor, offering effective anti-oxidant properties to suppress oxidative stress. By inhibiting the PI3K-Akt/NF-κB signaling pathway, chondrocytes protected by the tailored armor can secrete a cartilage matrix even in inflammatory microenvironments. In OA rat models, osteophyte formation and the inflammatory response have been inhibited by the cartilage-armor, demonstrating a therapeutic effect comparable to most drug-loaded systems. This study underscores the potential of tailoring cartilage-armor with the cartilage targeting and autophagy-activating properties in integrating offensive–defensive mechanisms for cartilage remodeling. This represents an alternative strategy for clinical OA therapy.

New concepts

The imbalance of offensive–defensive properties to osteoarthritis (OA) has severely affected joint lubrication. In this study, we proposed a new type of tailored cartilage-armor composed of lubricin–mimicking diblock copolymers. Unlike physical armor with weak binding to cartilage and chemical armor with insufficient anti-degradation, the tailored armor can target to damaged cartilage and provide durable lubrication, anti-degradation and anti-oxidation properties. In contrast to previous bioinspired lubricants, this armor exhibited an autophagy-activated antioxidation process to alleviate oxidative stress. Transcriptome analysis revealed that the tailored armor can facilitate the chondrogenesis of chondrocytes in an inflammatory microenvironment by downregulating the PI3K-Akt/NF-κB signaling pathway and upregulating the MAPK signaling pathway. Importantly, this tailored armor exhibited comparable therapeutic effects on OA rats to most drug-loaded systems, surpassing the effectiveness of traditional drugs and biomaterials. We believe that this innovative strategy offers a new approach for treating osteoarthritis and other inflammatory diseases.

1. Introduction

Osteoarthritis (OA) is a chronic disease characterized by the progressive degradation of the cartilage matrix, resulting in diminished capacity for joint lubrication.[1–3] The inherent lubricity of healthy cartilage relies on the continuous renewal of the cartilage matrix/synovial fluid, facilitating a notably low coefficient of friction (COF).[4,5] This low COF, attributed to boundary lubrication, minimizes shearing and dragging forces, thereby mitigating wear on the cartilage. However, individuals afflicted with OA due to aging or accident incidents face the inevitable damage of cartilage and chondral debris from the highlighted friction forces.[6,7] This phenomenon stimulates the secretion of metabolic enzymes and the overexpression of reactive oxygen/nitrogen species (ROS/RNS), further exacerbating the degenerative process.[4,6] In the context of OA, it becomes imperative to address the disruption of cartilage homeostasis, involving matrix regeneration and loss, especially within the inflammatory joints during the treatment of OA.[8,9]

[a] *College of Polymer Science and Engineering, State Key Laboratory of Polymer Materials Engineering, Med-X Center for Materials, Sichuan University, Chengdu 610065, P. R. China. E-mail: xiej@scu.edu.cn, fredca2005@163.com, jianshu_li@scu.edu.cn*
[b] *Experimental and Research Animal Institute, Sichuan University, Chengdu 610207, P. R. China*
[c] *Life Science Core Facilities, College of Life Sciences, Sichuan University, Chengdu 610065, P. R. China*
[d] *School of Aeronautics and Astronautics, Sichuan University, Chengdu 610207, P. R. China*
[e] *State Key Laboratory of Oral Diseases, West China Hospital of Stomatology, Sichuan University, Chengdu 610041, P. R. China*

† Electronic supplementary information (ESI) available: Detailed experimental materials and methods, including synthesis and characterization of lubricin–inspired polymers, investigation of cartilage-targeting, anti-oxidation, degradation resistance, cell studies and animal studies. See DOI: https://doi.org/10.1039/d4mh00812j

Generally, the treatment of OA is focused on the development of injectable polymers loaded with anti-inflammatory drugs or chondrogenic agents.[10–13] Notably, prevailing strategies emphasize the therapeutic effect of drugs over the polymers themselves. Recent advancements proposed biomaterials based on hyaluronic acid (HA), chondroitin sulfate (CS) and their derivatives, typically administered in the form of injectable micro/nanoparticles or hydrogels.[14–16] However, such a therapeutic approach for OA therapy is optimal as evidenced by the combinations of biomaterials and drugs, together with the side effects of frequent administration of drugs. Therefore, an alternative and potentially superior approach involves drug-free injectable biomaterials, aiming to establish a robust protective armor on the surface of the damaged cartilage. This strategy responds dynamically to changes in the synovial fluid compositions and cartilage matrix conditions. Consequently, the designed cartilage-armor serves to attenuate abnormal friction forces and prevent matrix degradation from ROS/RNS and degradation enzymes.

As for the molecular composition of cartilage-armor, a promising strategy involves the development of polymeric biomaterials inspired by substances in the cartilage matrix, notably CS and lubricin.[2,17] An inevitable challenge in the progression of OA is the impairment or disappearance of lubricin in the superficial layer of cartilage, which is the main reason for failure in effective lubrication.[18,19] To address this issue, the design of a lubricin-like polymer capable of lubricating the damaged cartilage surface is pursued. Hydrophilic block polymers, incorporating nonionic polyethylene glycol (PEG) and zwitterionic polyelectrolytes,[11,18–20] are commonly synthesized through controlled radical polymerization for this purpose. The robust binding of these polymers to cartilage, supported by aldehyde-bearing, *in situ* assembly, and ionic interactions, becomes imperative to ensure prolonged durability under conditions of frequent friction and within overactive joint microenvironments.[21–24] Compared to these methods, the utilization of cartilage-targeting peptides emerges as a potentially better choice due to their specific affinity to cartilage.[25,26] Notably, the WYRGRL hexapeptide, identified as a collagen type II (Col II)-binding peptide (ColBP),[22] demonstrates the ability to facilitate the specific binding forces to exposed Col II, particularly in the context of frictional wear. On the other hand, this hexapeptide features an oxidizable melatonin-like tryptophan residue (W) and a phenolic tyrosine residue (Y).[27] These chemically structural features suggest an ability to scavenge overexpressed free radicals in the OA environment, presenting a multifaceted therapeutic potential. To date, relevant work conjugating ColBP to zwitterionic polymers as tailored cartilage armors to restore lubrication performance, defend against the degradation process and relieve OA has rarely been reported.

Herein, we design a diblock poly(sulfobetaine)-*b*-poly(COLBP) (PSB-*b*-PColBP, denoted as PSP), drawing inspiration from lubricin that holds binding domains to proteins and brush-like lubrication domains (Scheme 1). PSP is engineered to create a tailored cartilage-armor *in situ* on the surface of damaged cartilage. This design is driven by the cartilage targeting properties of the peptide moiety and the hydrophilic properties of the zwitterionic moiety, respectively. By simulating the OA microenvironment, we quantify the anti-degradation capacity, targeted lubrication properties and anti-oxidation ability. Lipopolysaccharide (LPS)-activated inflammatory

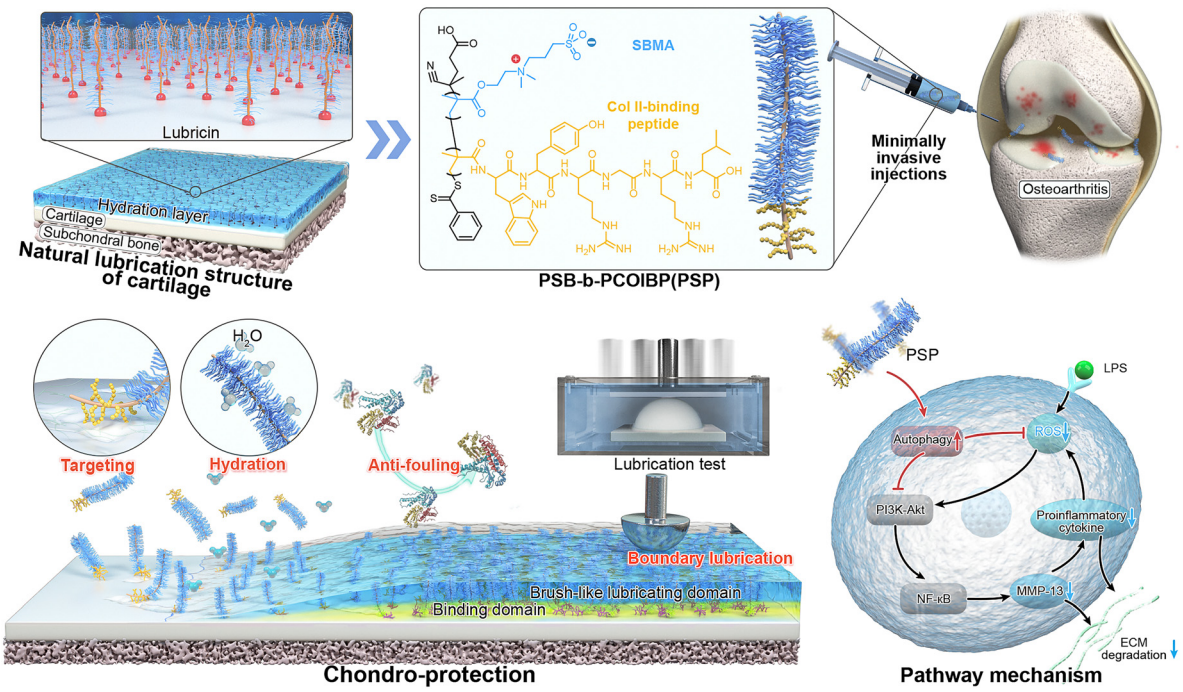

Scheme 1 Scheme of lubricin-inspired cartilage armor and its main functions including lubrication, anti-oxidation and enzyme resistance, which shows chondroprotective performance by activation of autophagy to alleviate OA.

environment is employed to clarify the ROS/RNS scavenging mechanism and correlation of "inflammation-PSP-chondrogenesis" by RNA sequencing (RNAseq) analysis. Furthermore, the therapeutic effect of PSP on OA rats has been evaluated by Micro-CT, histological and immunochemical staining, and RT-qPCR. We envision that this biomimetic cartilage-armor, which exhibits boundary lubrication, anti-degradation, ROS/RNS scavenging and anti-inflammatory abilities, will offer an alternative strategy for integrating offensive–defensive processes to promote cartilage remodelling for early OA therapy.

2. Results and discussion

2.1. Universal chemical cartilage-armor fails in chondroprotection properties

To enhance the adaptive chondroprotection properties of biomaterials in line with the intrinsic physicochemical properties of cartilage, various strategies have been proposed. One such strategy involves mimicking the structures of lubricin by synthesizing a diblock copolymer comprising a zwitterionic moiety and an active ester moiety (PSBMA-*b*-PNHSMA, PSN). The synthesis of PSN is achieved through two key steps: (i) modification of *N*-hydroxysuccinimide (NHS) with carbon–carbon double bonds to facilitate subsequent polymerization, offering high reaction activity with amino-containing molecules,[28] (Supplementary discussion S2.1 and Fig. S1, ESI†); (ii) the synthesis of PSN *via* reversible addition–fragmentation chain transfer (RAFT) polymerization (Fig. 1a).

The ^{1}H NMR spectra reveal that the actual ratio of reactive pendants to zwitterionic segments was approximately 1/10 (Fig. 1b). The elution times of PSB and PSN were 10.215 min and 10.087 min (Fig. 1c), respectively, indicating an increased molecular volume of PSN due to the introduction of NHS segments. The quantitative number-average molecular weight (M_n) values are 21 501 for PSB and 23 141 for PSN, respectively, implying that the molecular formula of the diblock copolymer is $PSBMA_{76}$-*b*-$PNHSMA_9$. Furthermore, the polydispersity index (PDI) values of 1.207 for PSB and 1.275 for PSN suggest a narrow molecular weight distribution. FT-IR analysis confirms the presence of sulfonyl groups (–S═O, 1036 cm^{-1} and 1180 cm^{-1}) and active ester groups (NHS, 1778 cm^{-1} and 1785 cm^{-1}) (Fig. S2, ESI†). XPS analysis

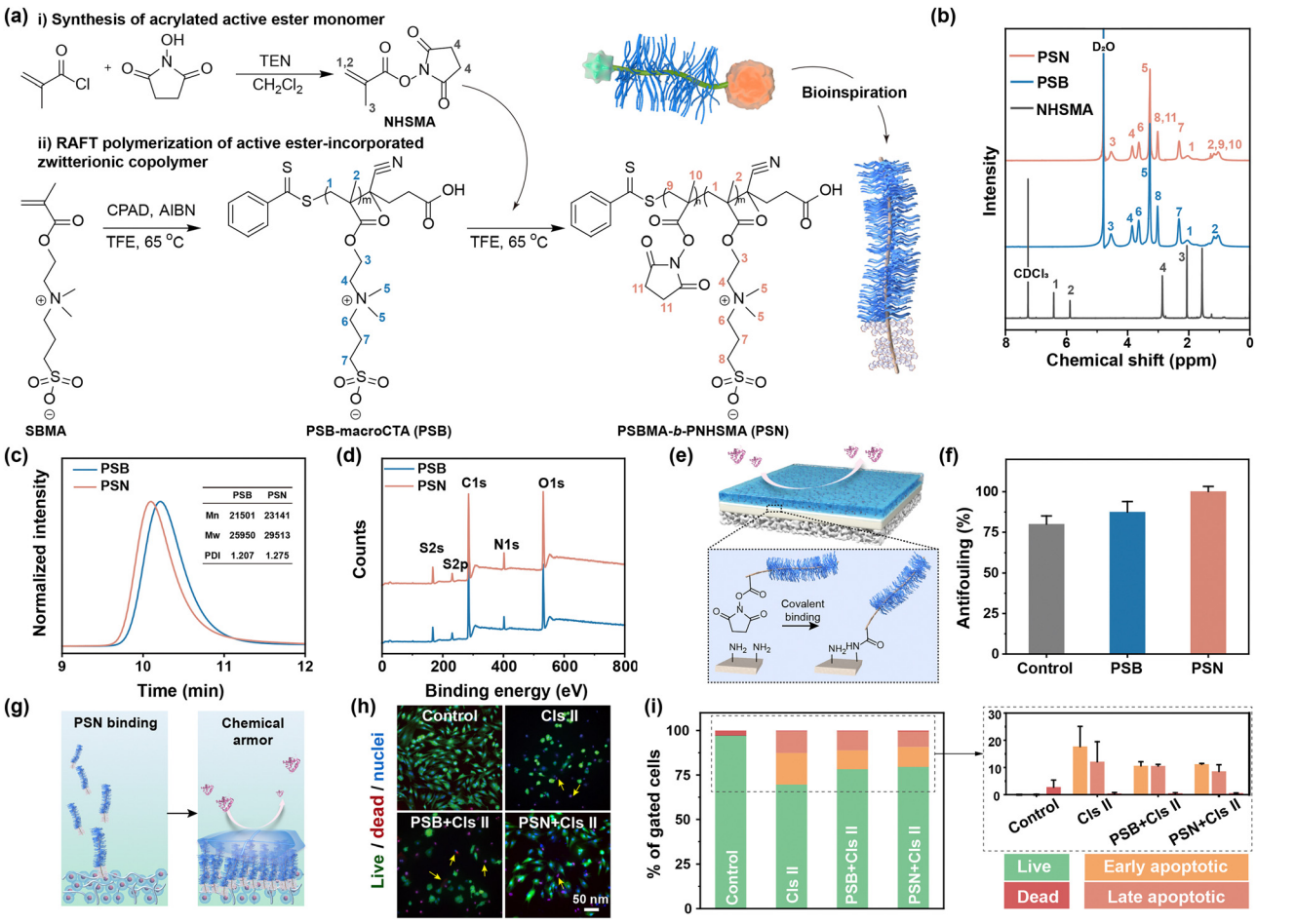

Fig. 1 The insufficient protection properties of universal chemical cartilage–armor. (a) The synthesis of the NHSMA monomer and lubricin-inspired PSN. (b) The 1H NMR, (c) GPC and (d) XPS spectra of PSB and PSN. (e) Scheme of the fabrication of chemical armor on the surface of cartilage disks and (f) the antifouling efficiency of modified cartilage. (g) Scheme of the construction of chemical armor in the microenvironment of chondrocytes. (h) Live/dead/nuclei staining images of chondrocytes with sequential armor formation and Cls II invasion, and (i) the corresponding cell states. The yellow arrows in (h) indicate the dead chondrocytes.

reveals that the N 1s signal is dominated by 88% of R–$N^+(CH_3)_3$ from PSB and 12% of N–C═O from PNHS (Fig. 1d and Fig. S3, ESI†), consistent with the above results. Meanwhile, thermogravimetric analysis indicates a delayed response after copolymerization with NHSMA (Fig. S4, ESI†), which can be attributed to the distinct thermodynamic properties between the sulfobetaine and the active ester moieties.

Resistance to enzymatic degradation of cartilage is an important criterion for effective OA therapy.[29] To develop a chemical cartilage armor, we obtained specimens from pig femurs and treated them with polymers. The robust covalent bonds form between the active ester groups of PSN and the amine groups on the cartilage surface, subsequently generating a hydration layer (Fig. 1e). There is negligible adsorption on the surface of cartilage with a chemical armor (Fig. 1f and Fig. S5, ESI†). To evaluate the protective property of this chemical cartilage armor in a more complex physiological environment, a specialized setup has been designed (Fig. 1g). Unfortunately, similar to weak physical cartilage-armor, the chemical cartilage-armor fails in inhibiting cell death and apoptosis induced by the degradation enzymes (Fig. 1h and i). In the microenvironment of chondrocyte growth, numerous amine-incorporated substances, such as amino acids and proteins, are present. PSN reacts with these substances due to the universal amide reactions (Scheme S1, ESI†), leading to reduced polymer conjugation to the extracellular matrix (ECM) and weakened chemical armor. Catabolic enzymes can easily traverse this polymer barrier, degrading the ECM and compromising the living environment of chondrocytes. Consequently, constructing a universal cartilage armor using an active ester-contained zwitterionic copolymer is insufficient for achieving the desired level of chondroprotection.

2.2. Tailored cartilage-armor inhibits enzymatic degradation

To improve polymer location at the cartilage matrix, a cartilage-targeted copolymer is synthesized through the conjugation of hexapeptide (WYRGRL) to PSN (Fig. 2a). The successful synthesis of this copolymer is confirmed by FT-IR, XPS, UV, FL, and CD analyses and using a BCA kit (Fig. S2, S6–S11 and Table S1 and Supplementary discussion S2.2, ESI†). The targeting ability of the copolymer is crucial for precise chondroprotection and prolonged retention time in the joint cavity, owing to its high affinity to cartilage.[30,31] The targeting efficiency (TE) of PSP to cartilage is a crucial factor in the context of OA treatment. Similar to the specific targeting property of WYRGRL hexapeptide towards Col II compared with CS and HA (Fig. S12 and S13 and Supplementary discussion S2.3, ESI†), PSP also demonstrate notable cartilage-targeting ability (Fig. 2b). This propensity is attributed to strong interactions such as hydrogen bonding (2.13 Å and 2.58 Å), C–H bonding (3.43 Å) and Pi–Pi interactions (3.79 Å and 4.80 Å). Furthermore, PSP's affinity to Col II (-6.41 kcal mol^{-1}) is found to be approximately 1.5 times higher than its affinity for HA (-3.83 kcal mol^{-1}) and CS (-3.94 kcal mol^{-1}) (Fig. 2c). Despite its tendency for spontaneous binding to HA, CS and Col II, PSP exclusively forms a stale complex with Col II (affinity < -5 kcal mol^{-1}).

To validate the targeting ability in complex microenvironments such as the chondrogenic extracellular matrix (ECM) and cartilage specimens, a reference pentapeptide (G_4D), lacking specific affinity to Col II, is conjugated to zwitterionic block polymer (PSB-*b*-PG_4D, named for "PSBG"). FITC-labeled polymer-peptide conjugates are incubated with 10^6 cells (Scheme S2, ESI†). Weak binding of both PSBG and PSP to SMSCs is observed (Fig. S14, ESI†), likely due to macromolecular interactions including ionic bonding, hydrogen bonding and van der Waals force. However, when incubated with BMSCs pretreated with chondrogenic induction medium, PSP demonstrated a TE of 33.29%, which is 2.26-fold higher than that of PSBG. Moreover, PSP exhibits the highest TE towards chondrocytes (54.09%), known for secreting Col II. Statistically, the TE of PSP towards chondrocytes is 4.21-fold higher than that of PSBG ($p < 0.05$). These data indicate that Col II-rich entities, including Col II fragments, C-BMSCs, and chondrocytes, are the precise targets of PSP, thereby providing chondroprotection properties for subsequent OA therapy.

Due to the specific affinity of hexapeptide (WYRGRL) to abundantly exposed Col II in damaged cartilage, PSP copolymer exhibits a targeted localization to the cartilage surface. This location forms a dense hydration armor *in situ* through ionic interactions and hydrogen bonds facilitated by the brush-like PSB moiety (Fig. 2d). In the case of pristine cartilage disks from pigs, they absorb FITC-BSA on the surface through multiple interactions such as hydrogen bonds and hydrophobic interactions. Consequently, there is little residual FITC-BSA in the incubation solution, leading to a reduction in the FL intensity (Fig. S15, ESI†) and an undesirable anti-fouling efficiency (Fig. 2e). In contrast, cartilage disks pretreated by PSP exhibit a nearly 100% reduction in BSA adsorption. This reduction is attributed to the synergistic effect of targeting capacity and hydrophilic properties of PSP. The tailored armor also supports chondrocyte growth in the simulated microenvironment. After sequential armor fabrication and incubation with catabolic enzymes such as hyaluronidase (Hyase) and collagenase II (Cls II), the cell state is evaluated by live/dead/nuclei staining. Chondrocytes treated with Cls II exhibit a shift from a spread morphology to a rounded shape, accompanied by cell death. PSB shows an almost non-chondroprotective effect, while the tailored armor has effectively inhibited cell apoptosis and death (Fig. 2f). The tailored armor also prevents degradation invasion of Hyase toward chondrocytes (Fig. S16, ESI†). Flow cytometry reveals a reduction in apoptotic chondrocytes from 29.90% with Cls II treatment to 19.83% and 0.05% with the protection of PSB and PSP, respectively (Fig. S17, ESI†).

The *in vivo* anti-degradation effects of the tailored cartilage-armor are evaluated systematically. After the intra-articular (I.A.) injection of Cls II, the cartilage surface appears discontinuous and rough, showing no improvement in the PSB group due to its lack of effective cartilage-binding ability to form a protective layer, as demonstrated by H&E staining (Fig. S18, ESI†) and Masson's staining (Fig. 2g) images. Remarkably, the PSP group exhibits no discernible difference from the normal group, owing to the excellent anti-fouling property of the tailored cartilage-armor. Additionally, the tailored armor effectively protects the

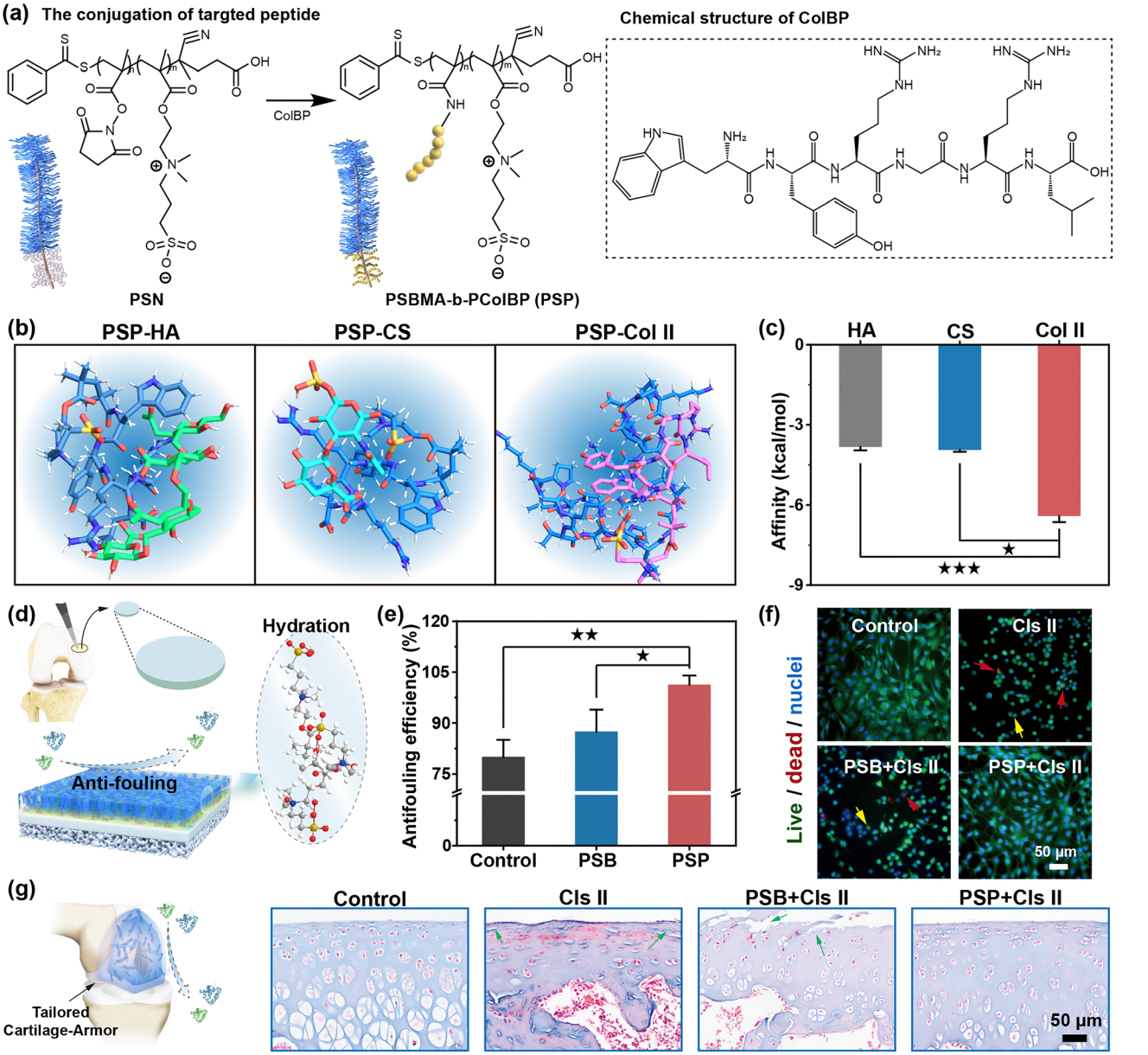

Fig. 2 Tailored cartilage armor exhibits anti-degradation properties. (a) Scheme of the synthesis of cartilage-targeted zwitterionic PSP. (b) Molecular docking and (c) the corresponding affinity between PSP and biomacromolecules rich in the cartilage matrix (HA, CS and Col II). (d) Scheme of fabrication of tailored hydration armor on the surface of cartilage disks and the (e) antifouling efficiency of modified cartilage. (f) Live/dead/nuclei staining images of chondrocytes with sequential treatments of armor formation and CIs II invasion. (g) The degradation resistance effect of tailored armor. ★($p < 0.05$), ★★($p < 0.01$) and ★★★($p < 0.001$) indicate significant differences.

cartilage against Hyase. The anti-degradation effect of PSP is further proved by the maintenance of HA and Col II in the cartilage matrix (Fig. S19–S21 and Supplementary discussion S2.4, ESI†). These results indicate that PSP, targeting Col II to generate a hydration armor, maintains the survival ratio of chondrocytes and the normal cartilage structure by repelling the adsorption of catabolic enzymes. The prominent fouling resistance of the tailored cartilage-armor involves the hydration effect and steric hindrance effect. The former, owing to the ion–dipole interactions with water molecules, provides the targeted PSP high hydration capacity to generate a compact layer, which diminishes the adhesion of degradation enzymes through ionic bonds and hydrophobic interactions. The latter is related to the change in Gibbs free energy, $\Delta G = \Delta H - T\Delta S$.[32] The isothermal process of adhesion of degradation enzymes reduces the entropy of the surface system of PSP-targeted cartilage, causing $\Delta G > 0$. Therefore, the polymer armor repels the degradation enzymes, further preventing cartilage damage.

2.3. Durable biolubrication of the tailored cartilage-armor

Growing evidence highlights the pivotal role of lubrication in mitigating cartilage surface wear.[33,34] Therefore, the targeted

lubrication properties of PSP directly influence the wear resistance of cartilage. In a ball-to-plate test, the COF of PSP is consistently lower than that of PSB, irrespective of loading forces and sliding frequency (Fig. S22 and Supplementary discussion S2.5, ESI†). However, it is imperative to note that this test method diverges from the articular movement of cartilage, as the interactions between polymers and Al_2O_3 ball or PTFE plate are inherently weak. To address this limitation, a self-developed model has been applied to investigate the targeted lubrication properties of PSP (Fig. 3a). In this *ex vivo* model, PSP displays a TE towards the cartilage surface almost 3.1-fold higher than that of PSBG ($p < 0.01$) (Fig. 3b), thereby inducing the formation of a cartilage-armor. The untreated samples show the highest COF at 0.043–0.063. PSBG modification marginally reduced the COF, while the samples with tailored cartilage-armor consistently exhibited the lowest COF at all frequencies (0.5, 1.0 and 1.5 Hz) (Fig. 3c–e and Fig. S23, ESI†). These differences align with the TE of PSBG and PSP. Similar results could be also observed using femoral condyle as test samples (Scheme S3, Fig. S24 and Supplementary discussion S2.6, ESI†).

To explore the stability of the targeted lubrication of PSP, 500 sliding cycles have been carried out. After approximately 100 cycles, the COF of PSBG-treated cartilage gradually increases (Fig. 3f), whereas PSP-targeted cartilage maintains efficient lubrication with a COF consistently below 0.013. In the initial stages of the lubrication test (<50 cycles), both PSBG and PSP could peel off from the cartilage's surface, possibly due to weak bonding with the biomacromolecules of the cartilage ECM. However, the gradually increased FL intensity of PSBG in the sliding solution reveals unstable polymer association under the dynamic conditions and failure in long-term lubrication (Fig. 3g). After nearly 400 cycles, there is a slight increment in the FL intensity of PSP, but this change has no discernible

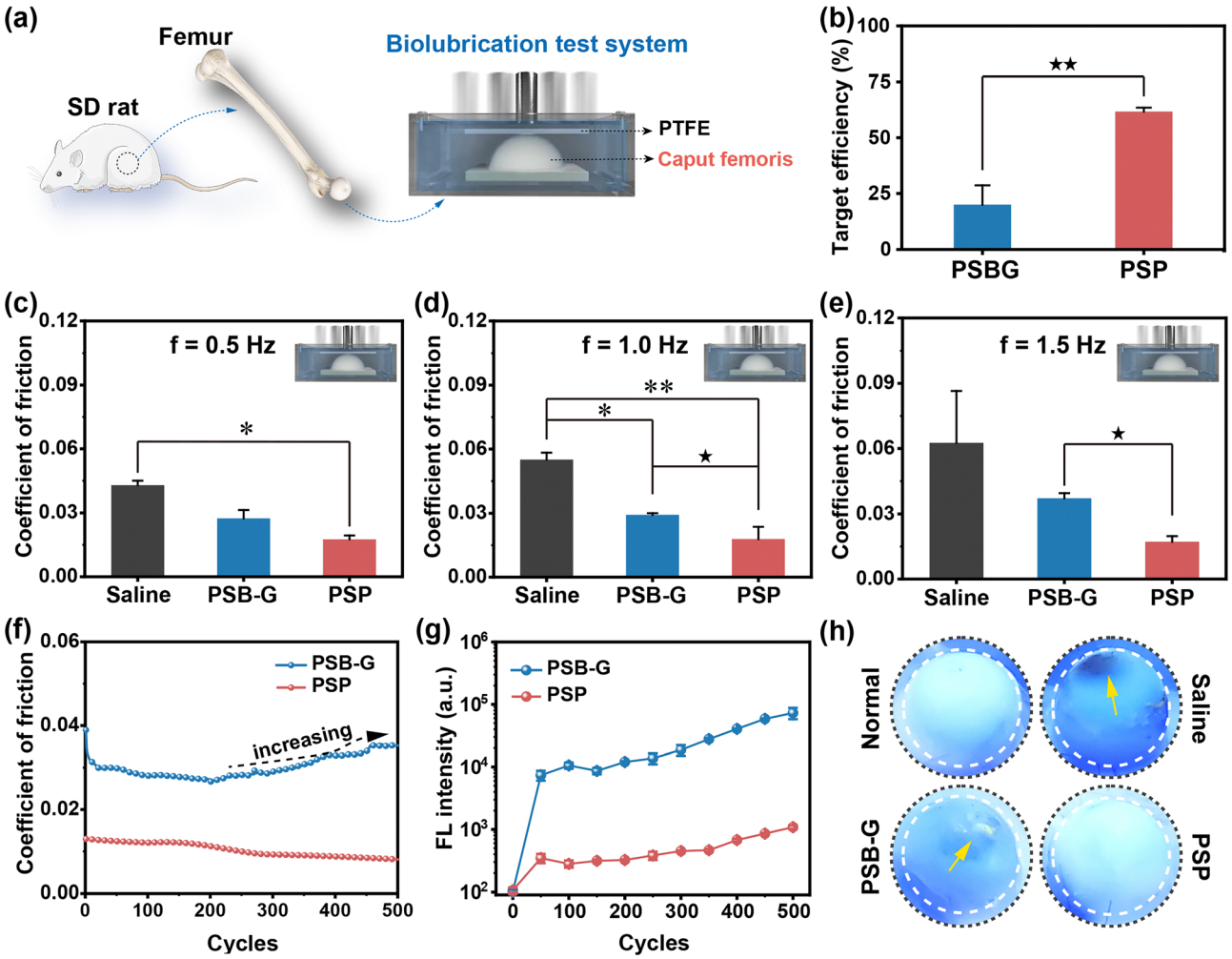

Fig. 3 The specifically targeted lubrication properties of tailored cartilage–armor. (a) Scheme of collection of caput femoris and the lubrication test. (b) The target efficiency of PSBG (a reference with invalid targeting efficiency) and PSP toward *ex vivo* cartilage specimens. The coefficient of friction of cartilage with tailored armor at frequencies of (c) 0.5 Hz, (d) 1.0 Hz and (e) 2.0 Hz, respectively. (f) The change in the coefficient of friction of PSP-targeted cartilage under 1.0 Hz with 500 cycles. (g) The fluorescence intensity of solutions at different time points under the lubrication test and (h) the visual images of cartilages after the lubrication test. The yellow arrows represent the wear of cartilage. *($p < 0.05$) refers to the statistical difference in comparison to the control (or saline) group. ★($p < 0.05$), ★★($p < 0.01$) and ★★★($p < 0.001$) indicate significant differences.

impact on the COF. Like pristine cartilage undergoing serious wear damage in saline during the lubrication test, obvious scars appear on the surface of PSBG-treated cartilage due to its frictionally intolerable properties (Fig. 3h). In contrast, PSP-targeted cartilage exhibits an intact and smooth surface. In essence, the copolymer absorbs water molecules through hydrogen bonds to form a hydration armor, further strengthened by condensed networks through strong electrostatic interactions of ionic pairs and multiple hydrogen bonds. Consequently, the targeted PSP application on the cartilage surface contributes to its excellent anti-friction properties, offering a promising potential for enhanced lubrication and wear resistance in the context of OA therapy.

2.4. Anti-oxidation properties of the tailored cartilage-armor

In the OA joint, chondrocytes are subjected to abnormal oxidative stress,[35] initiating a cascade enzymatic catalysis that results in the substantial generation of ROS/RNS (Fig. 4a). The excessive production of free radicals involves dysregulated articular inflammatory response, triggering the secretion of degradation enzymes, cell apoptosis and necrocytosis.[36,37] Consequently, anti-oxidant therapy tends to be a promising approach to alleviate OA.

2.4.1. ROS scavenging. The overexpression of superoxide anion ($O_2^{\bullet-}$) in the joint can induce the destruction of the cartilage matrix, DNA damage and degradation of HA in the synovial fluid.[8] This deleterious effect can be naturally mitigated by superoxide dismutase (SOD).[38] PSB demonstrates only

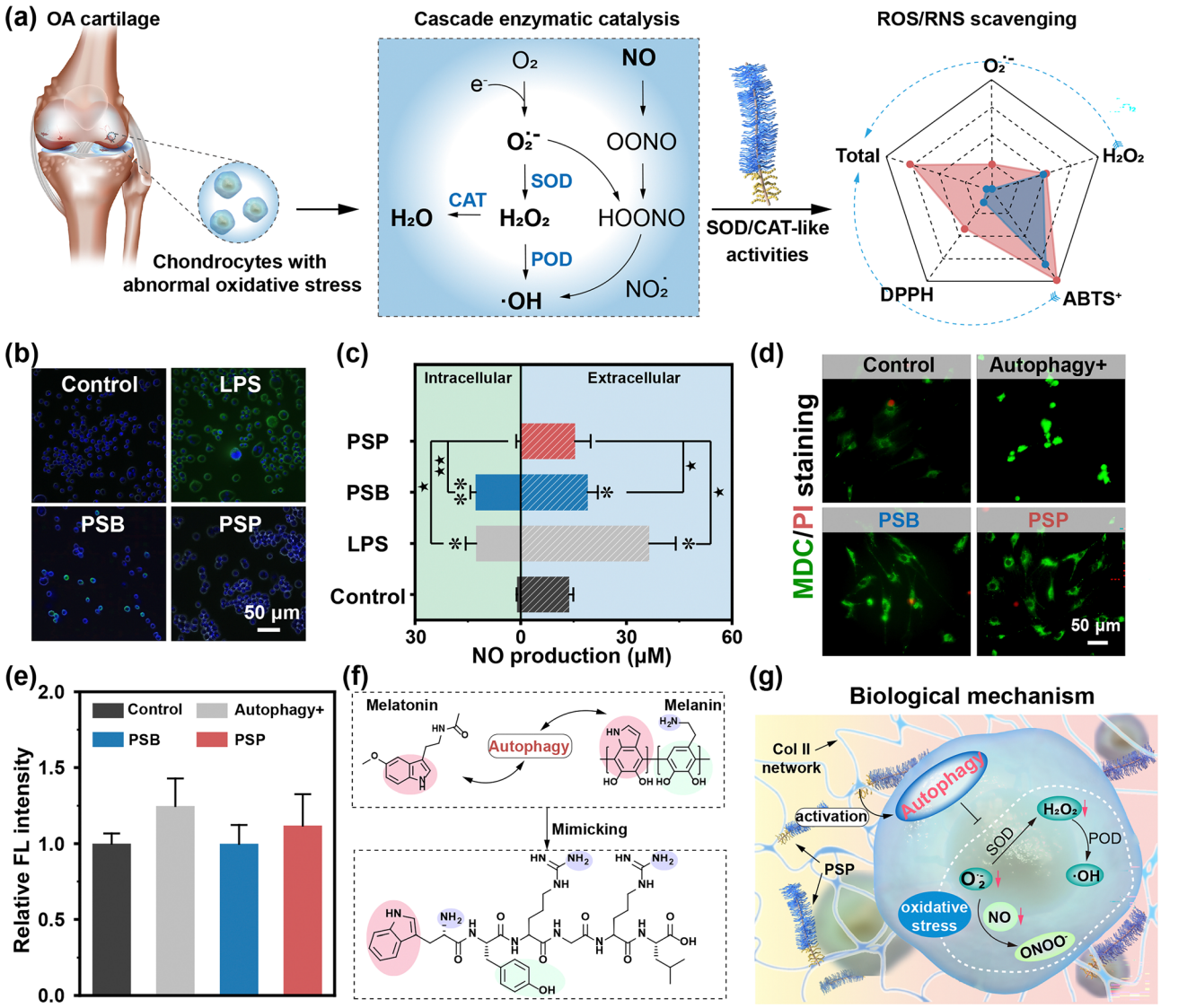

Fig. 4 The anti-oxidant property of PSP. (a)The cascade enzymatic catalysis in chondrocytes in the OA joint and the antioxidase-like activities of PSP. (b) The intracellular NO staining and (c) the quantitative analysis of extracellular and intracellular NO production. *($p < 0.05$) and **($p < 0.01$) refer to significant differences compared with the control group. ★($p < 0.05$) and ★★ ($p < 0.01$) indicate statistical differences between other groups. (d) The MDC/PI staining images. The green color indicates cells with activated autophagy, and the red spots represent dead cells. (e) Their corresponding relative FL intensity of cells incubated with PSB and PSP. (f) The potential effect of PSP on autophagy activation through similar chemical structures to melatonin and melanin. (g) The biological mechanism of the autophagy-mediated anti-oxidation property of PSP.

an $O_2^{\bullet-}$ scavenging ratio of 1.97% (Fig. S25, ESI†), which is not significantly different from the control group and is considered ineffective. Following peptide conjugation, PSP shows a statically 12.20-fold higher scavenging ratio ($p < 0.001$), suggesting excellent improvement of SOD-like activity. Regarding the CAT-like activity of PSP to scavenge H_2O_2, which keeps relatively stable at high levels in inflamed joints, $Ti(SO_4)_2$ is used to capture the H_2O_2 molecules. Compared to the H_2O_2 solution, the addition of both PSB and PSP results in reduced residual H_2O_2 concentration (Fig. S26, ESI†). The H_2O_2 scavenging of PSP is calculated to be 51.04%, which is higher than that of PSB (48.41%). Furthermore, hydroxyl radical ($^{\bullet}OH$) is another representative ROS that accelerates the progression of OA,[39] reacting with pure terephthalic acid (PTA) and displaying high fluorescent intensity at 425 nm. There is lower FL intensity in both PSB and PSP groups compared to the H_2O_2 group (Fig. S27, ESI†), considered a positive reference since H_2O_2 tends to decompose into abundant $^{\bullet}OH$. Moreover, compared with PSB, the further reduction in FL intensity of PSP demonstrates better $^{\bullet}OH$ scavenging ability. Additionally, PSP also exhibits scavenging ability toward PTIO, another indicator of ROS (Fig. S28, ESI†).

2.4.2. RNS scavenging. As for RNS scavenging, $ABTS^+$ and DPPH are selected as two representative indicators to evaluate the scavenging ability of PSB and PSP. Briefly, ABTS reacts with $(NH_4)_2S_2O_8$ to generate aquamarine blue $ABTS^+$ radicals, which are subsequently decolorized by anti-oxidants (Fig. S29, ESI†). The incorporation of ColBP is an important enhancement to improve the limited scavenging ability of PSB to $ABTS^+$ (81.19%), emphasizing the higher scavenging ratio of PSP (98.65%). In addition, the single electron of DPPH is captured by the anti-oxidants (PSB and PSP), leading to fading of the purple color and a decrease in the maximum wavelength at 517 nm decreases (Fig. S30a–c, ESI†). Significantly, compared to PSB, the scavenging ratio of DPPH in the PSP group has increased by 3.27-fold ($p < 0.001$, Fig. S30d, ESI†). The notable RNS scavenging ability of PSP lays the foundation for relieving abnormal oxidative stress and further suppressing the inflammatory response.

2.4.3. The synergistic anti-oxidant mechanism of anti-oxidase-mimicking activities and autophagy-activation. The tryptophan residue in the ColBP exhibits a similar β-indole group to melatonin and melanin, facilitating electron/proton transfer for scavenging ROS, especially superoxide radical (Scheme S4a, ESI†). Another important cue in ColBP is the tyrosine residue with a phenol group. Through a hydrogen atom donation process and electron transfer-proton transfer, the reversible transformation between the phenol group and quinone group continuously scavenges oxygen and nitrogen radicals (Scheme S4b and c, ESI†). In addition, similar to the lipid oxidation process, the reactive methylene groups in the PSB act as sacrificial moieties for eliminating free radicals (Scheme S4d, ESI†). Consequently, PSP exhibits better performance in ROS/RNS scavenging (Fig. 4a), and its total antioxidation activity is 14.83-fold higher than that of PSB ($p < 0.05$, Fig. S31, ESI†), implying that conjugation of ColBP is comprehensively superior to homopolymerized PSB in the OA joint with elevated oxidative stress.

Utilizing the anti-oxidation performances as a foundation, we characterized the anti-oxidation abilities of PSP towards macrophages and normal tissue cells, investigating potential biological mechanisms. Upon LPS stimulation, inflammatory responses are activated, thereby producing a substantial amount of $^{\bullet}OH$ and $O_2^{\bullet-}$ (Fig. S32, ESI†). The residual FL intensity of the PSB group demonstrates that PSB lacks the ability to scavenge intracellular $^{\bullet}OH$ and $O_2^{\bullet-}$ completely. Following ColBP conjugation, there are virtually no fluorescent signals in the PSP group. NO, reacting with $O_2^{\bullet-}$ to generate RNS, is shown to have its activated green fluorescence weaken when incubated with PSP rather than PSB (Fig. 4b). Moreover, quantitative analysis of intracellular and extracellular NO production shows effective inhibition by PSP of LPS-activated NO production (Fig. 4c). The anti-oxidation capacities of PSB and PSP are further investigated in normal joint cells, including chondrocytes, BMSC and SMSCs, showing results consistent with those of RAW264.7 cells (Fig. S33–S35, ESI†). PSP not only inhibits the overproduction of ROS/RNS inside macrophages but also eliminates free radicals inside normal cells. Different from the chemical analytic method, cellular antioxidation behaviors are found to extend beyond chemical reactions, potentially involving biological mechanisms. Autophagy, a "self-eating" process regulating energy metabolism and restoring mitochondrial functions,[25,40] emerges as a potential route for eliminating intracellular ROS/RNS. MDC/PI staining images reveal higher green FL intensity in the autophagy-activated group ("Autophagy+") compared to the control group (Fig. 4d and e). PSB exhibits lower FL intensity than that of the "Autophagy+" group, indicating that zwitterionic PSB alone does not induce autophagy behavior. PSP, on the other hand, demonstrates enhanced FL intensity, indicating that the introduction of ColPB not only contributes to targeting ability but also induces cellular anti-oxidations through activated autophagy behavior. Similar results are confirmed in bone mesenchymal stem cells (BMSCs) and synovial-derived mesenchymal stem cells (SMSCs) (Fig. S36, ESI†). Attenuation of the anti-oxidation system in an inflammatory microenvironment leads to overexpressed intracellular ROS/RNS and subsequent damage to protein and lipid molecules, underscores the rationale for activating autophagy to mitigate the side effects. PSP is therefore recognized as an autophagy inducer to switch on the intracellular self-defensive mechanism. Overall, the excellent anti-oxidation properties of PSP are supported through two routes: (i) intrinsic enzyme-like (especially SOD-like) activity, mainly provided by the Trp and Tyr, effectively scavenging the intracellular and extracellular ROS/RNS; and (ii) activated autophagy inhibiting ROS/RNS production and preventing oxidative damage (Fig. 4f and g).

2.5. The tailored cartilage-armor facilitates chondrogenesis

2.5.1. RNA-seq analysis. Prior to further investigation of biofunctions, the biocompatibility of PSP is confirmed through desirable cell viability and proliferation (Supplementary discussion 2.7, ESI†), extremely low dead/live ratios, and a spread cell morphology (Fig. S37–S39, ESI†). Additional indicators, including normal LDH release (Fig. S40, ESI†) and low apoptosis ratios (Fig. S41, ESI†), further confirm the favorable biocompatibility of PSP.

Moreover, PSP demonstrates the ability to support cell growth even under simulated inflammatory conditions (Fig. S42, ESI†). To elucidate the molecular mechanisms underlying the inflammation inhibition and chondrogenesis promotion associated with lubricin-inspired PSP, we have conducted RNAseq bioinformatic analysis. The gene expression profiles are compared between the LPS-induced group and the group treated with PSP following LPS induction (Fig. 5a). In the PSP group, 625 differently expressed genes (DEGs) ($p_{adj} < 0.05$ and |fold change| > 2, Fig. 5b) are identified, comprising 255 for up-regulated and 370 for down-regulated DEGs, compared to the LPS group.

Functional enrichment analysis, encompassing Gene Ontology (GO) and Kyoto Encyclopedia of Genes and Genomes (KEGG), is performed to gain insights into the role of these DGEs. The GO enrichment analysis of up-regulated DGEs reveals involvement in glycosaminoglycan binding, ''oxidoreductase activity'', cartilage development, response to lipopolysaccharide, chondrocytes differentiation and chondrocyte development (Fig. 5c), indicating concurrent LPS-inductive inflammatory response and cartilage regeneration. Conversely, the down-regulated DGEs in GO enrichment analysis are associated with glycosaminoglycan binding, cartilage development, response to lipopolysaccharide, positive regulation of inflammatory response and regulation of the Wnt signaling pathway, suggesting the suppression of inflammation progression alongside cartilage regeneration (Fig. 5d).

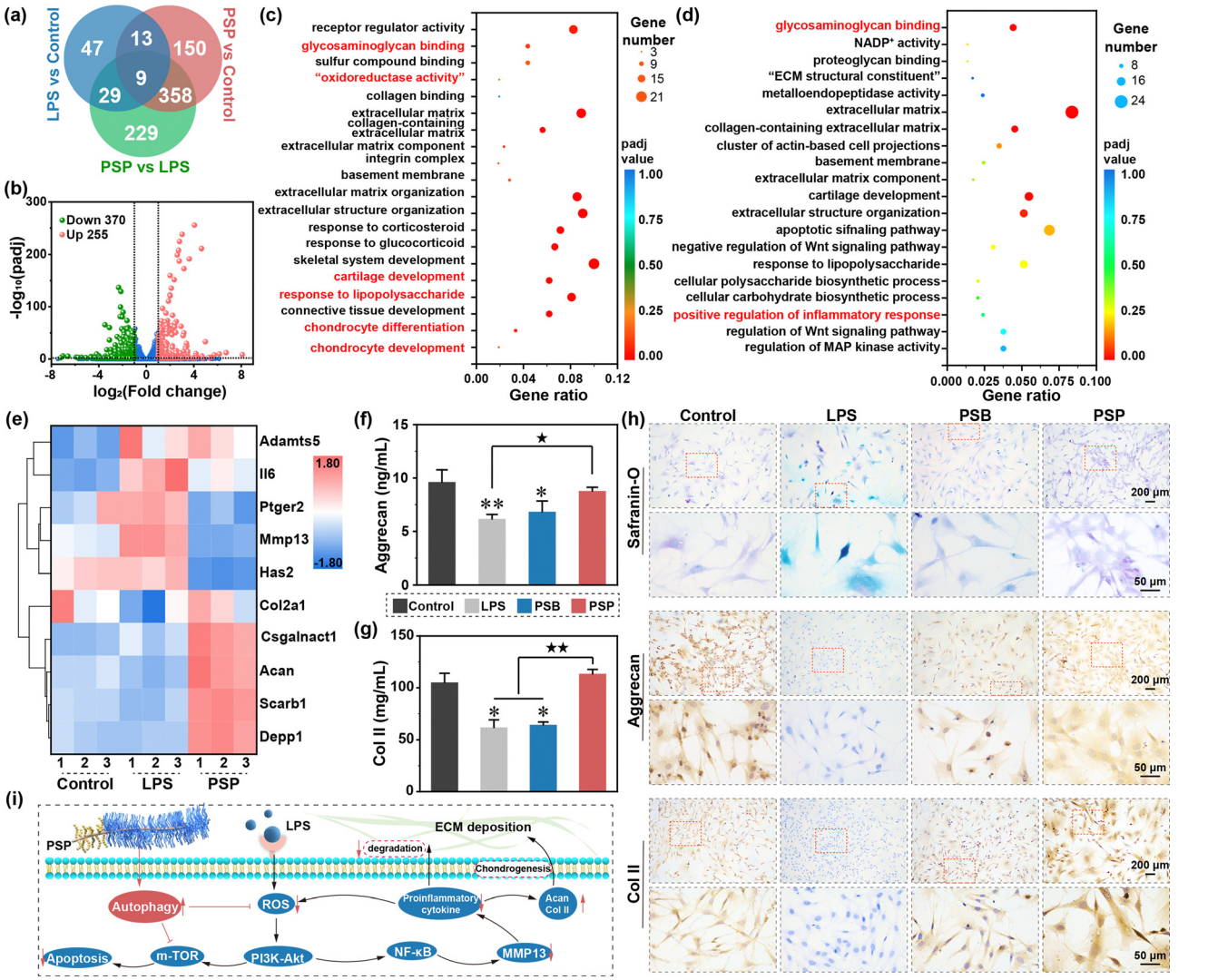

Fig. 5 Chondroprotection capacity of PSP in inflammation inhibition. (a) Veen diagram of DGEs common to all three gene expression omnibus (GEO) datasets. (b) Volcano plot of DEGs between PSP and LPS groups. GO enrichment analysis of (c) up-regulated and (d) down-regulated DEGs. The ''oxidoreductase activity'' in (c) is ''oxidoreductase activity, acting on paired donors, with incorporation or reduction of molecular oxygen, NADPH as one donor, and incorporation of one atom of oxygen''. The full explanation of ''ECM structural constituent'' in (d) is the ''extracellular matrix structural constituent''. (e) Heatmap of hierarchical cluster analysis of DGEs of interest. The quantitative protein expression of (f) Aggrecan and (g) Col II through ELISA assay kits. *($p < 0.05$) and **($p < 0.01$) suggest significant differences in comparison to the control group; ★($p < 0.05$) and ★★($p < 0.01$) indicate statistical difference among other groups. (h) Safranin O, aggrecan and Col II staining of control, LPS, PSB and PSP groups. (i) The regulatory effect of PSP on the signalling pathways related to autophagy, inflammation, apoptosis and chondrogenesis.

KEGG enrichment analysis of upregulated DEGs reveals involvement in glycosaminoglycan biosynthesis-chondroitin sulfate/dermatan sulfate and Toll-like receptor signaling pathways, confirming the chondrogenic potential of PSP (Fig. S43, ESI†). Notably, the ''autophagy-others'' pathway is highlighted, aligning with the anti-oxidant property discussed earlier. Down-regulated DEGs in KEGG enrichment analysis refer to inflammatory processes, such as the PI3K-Akt signaling pathway, the p53 signaling pathway, inflammatory mediator regulation of TRP channels and the Toll-like receptor signaling pathway (Fig. S44, ESI†). Additionally, the down-regulated DEGs in KEGG enrichment analysis are linked to apoptosis, reinforcing PSP's inhibitory effect on cell apoptosis under inflammatory conditions. Collectively, these data imply that PSP shows a positive effect on anti-inflammation and chondrogenesis. Hierarchical cluster analysis of ten DGEs of interest (Fig. 5e) further supports the roles of PSP in alleviating inflammation, promoting chondrogenesis and activating autophagy. These results are also confirmed by RT-qPCR (Fig. S45, Supplementary discussion S2.8, ESI†).

2.5.2. The cartilage-armor regulates the expression of inflammation-related and chondrogenesis-related proteins. In addition to its inhibitory effect on MMP-13 and adamts-5 expression, PSP also demonstrates the ability to suppress the secretion of interleukin-6 (IL-6), prostaglandin-2 (PGE-2) and tumor necrosis factor-alpha (TNF-α) (Fig. S46 and Supplementary discussion S2.9, ESI†). Anabolic processes are crucial for the formation of the cartilage matrix. Under LPS induction, there is a significant reduction in the expression of aggrecan ($p < 0.01$) and Col II ($p < 0.05$), and PSB shows no efficacy in reversing these adverse effects (Fig. 5f and g). In contrast, PSP provides multiple protection of PSP, resulting in a 1.42-fold increase in aggrecan secretion and a 1.84-fold increase in Col secretion compared to the LPS group, equivalent to the control group. Safranin O-fast green (SF) staining shows reduced expression of anionic aggrecan after LPS stimulation. While PSB exhibits limited effectiveness with lighted coloration than the control group, chondrocytes protected by PSP show significant improvement in chondrogenesis (Fig. 5h). These results are further supported by PAS and AB staining (Fig. S47, ESI†), suggesting that PSP facilitates chondrocytes in producing glycosaminoglycan and hyaluronic acid in the inflammatory microenvironment. Immunohistochemical staining of aggrecan and Col II is conducted to confirm the chondroprotective property of lubricin-inspired cartilage-targeted PSP. Normal chondrocytes secrete abundant aggrecan and Col II. However, these features are disrupted in the LPS and PSB-treated groups. As for chondrocytes treated with PSP, the expression of aggrecan and Col II is re-upregulated, as confirmed by the semi-quantitative analysis by gray value calculations (Fig. S48–S49, ESI†). These results indicate that lubricin-inspired cartilage-armor effectively maintains the normal chondrogenesis process in inflammatory condition, suggesting great potential in healing OA.

2.5.3. The biological mechanism of cartilage remodeling by the tailored cartilage-armor. In inflammatory microenvironments, the upregulation of ROS/RNS activates the PI3K-Akt signaling pathways. Subsequently, this activation further stimulates the downstream mTOR signaling pathway, leading to induce cell apoptosis.[41] Simultaneously, the activated PI3K-Akt signaling pathway positively influences the NF-κB signaling pathway, thereby initiating an inflammatory response.[42] Autophagy, induced by PSP, exerts a counteractive effect on ROS/RNS generation and the mTOR signaling pathway, establishing a negative feedback regulation loop toward the PI3K-Akt signaling pathway (Fig. 5i). Consequently, the expression of pre-inflammation genes (MMP-13 and Adamts-5) is suppressed, ensuring the normal expression of chondrogenic genes (Acan and Col II) and reducing ECM degradation in the inflammatory conditions. This orchestrated regulatory mechanism highlights the multifaceted impact of PSP on inflammation and chondrogenesis in the context of OA.

2.6. The cartilage-armor relieves OA through its chondroprotective abilities

2.6.1. The tailored cartilage-armor reconstructs the damaged cartilage. Currently, numerous studies focus on OA therapy utilizing zwitterionic polymer systems for reducing COF and delivering anti-inflammatory drugs.[43–45] In order to substantiate the distinct advantages of cartilage-target drug-free cartilage-armor more convincingly, we have conducted an OA model induced by ACLT surgery to evaluate the therapeutic effects of PSP (Fig. 6a). Osteophytes, absent in the normal group, are markedly present in the OA group (Fig. 6b). PSB injection doesn't exhibit a therapeutic effect on inhibiting osteophyte formation, even though the damaged area appears smaller. In contrast, PSP treatment effectively reduced osteophytes by 29.5% (Fig. 6c). The rough and inconsecutive surface of cartilage indicates that the movement of joints with insufficient biolubrication would induce obvious cartilage abrasion. PSB in the joint cavity cannot generate robust cartilage-armor, thus it fails to reduce friction forces and results in cartilage wear. The tailored cartilage-armor generated from targeted PSP could provide low COF, thereby inhibiting the cartilage damage (Fig. 6d). The full-layer structures of cartilage are also evaluated by Masson's staining. As shown in Fig. 6e, there are obvious intermitted surface and disrupted gradient structures in the OA group. PSB treatment, despite showing certain lubrication properties, does not completely break down cartilage, and the aggregated cells on the surface indicate the cartilage is within the period of healing. In contrast, PSP treatment results in the regeneration of intact and smooth hyaline cartilage. These data imply that the tailored armor for cartilage is able to promote cartilage regeneration in the OA joint.

Col II is one of the major cartilage components, and its secretion and deposition serve as a direct index for evaluating OA therapy (Fig. 7a). Immunohistochemical staining of Col II indicates massive Col II loss in the OA and PSB groups, while abundant Col II expression is observed in the PSP group. The expression of proteoglycan is characterized by safranin O-fast green staining. In comparison to the normal cartilage rich in proteoglycan expression (red matrix), there is only associated fast green to collagen (green matrix) in the OA group, which is

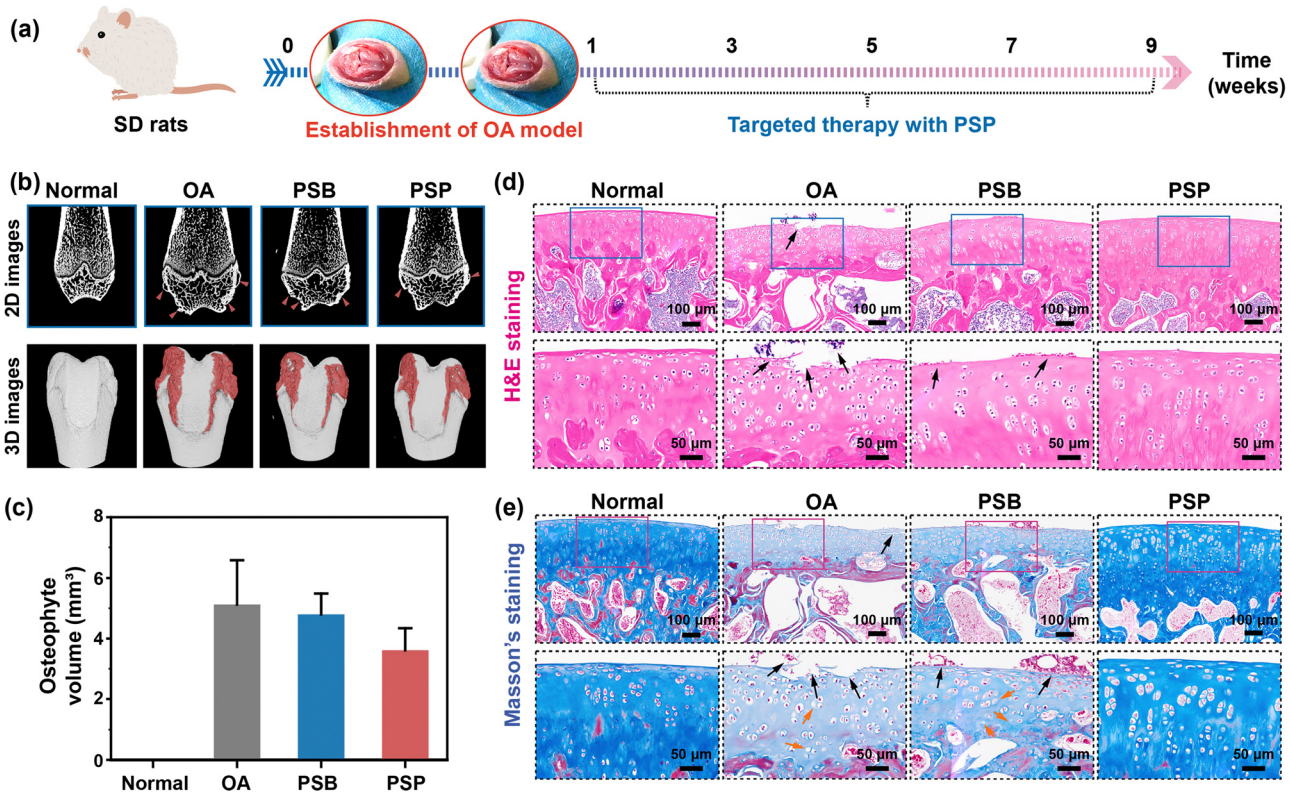

Fig. 6 Targeted OA therapy of tailored cartilage armor. (a) Schedules of OA surgery and PSP treatment. (b) 2D images and reconstructed 3D structures of femurs, (c) osteophyte volumes, (d) H&E staining and (d) Masson's staining images of normal, OA, PSB and PSP groups. Black arrows in (d) and (e) suggest fissures of cartilage or clusters of cells. Orange arrows in (e) suggest the absence of chondrocytes.

due to the degradation of anionic proteoglycan by OA (Fig. 7b). Owing to the weak chondroprotective properties of PSB, the proteoglycan degradation has been suppressed tightly while the red color of the cartilage matrix is also lighter than that of the normal group. PSP can form an *in situ* armor on the surface of cartilage with comprehensive chondroprotective capacities, thus the expression of proteoglycan is similar to the normal groups. The quantitative analysis of the OARSI score is summarized by the histological staining images. It is obvious that the OA group and PSB group with ineffective OA therapy have higher OARSI scores than that of the normal group ($p < 0.01$). With the introduction of the tailored cartilage-armor, the OARSI score has significantly reduced, which is equal to the normal group (Fig. 7c). Similarly, the Mankin score has confirmed the advanced effect on OA therapy in terms of cartilage structures, cells, matrix compositions and total evaluations (Fig. S50, ESI†). ICRS (macroscopic appearance; Fig. S51, ESI†) also indicates that PSP exhibits a superior therapeutic effect compared to PSB. Taking the reduction of OARSI score as an evaluation index, the therapeutic efficacy of PSP without and addition of drugs surpasses that of drugs, HA-based injection formulation and other injectable polymer systems. Moreover, it can reach the upper limit of drug-loaded polymeric systems (Fig. 7d). Joint homeostasis of catabolic and anabolic processes is further confirmed by RT-qPCR. As shown in Fig. 7e, relative adamts-5 expression is significantly increased in OA ($p < 0.01$) and PSB ($p < 0.05$) compared to the normal group, with PSP showing significantly lower adamts-5 expression than the OA group ($p < 0.05$). Similarly, MMP-13 expression is lower in both PSB and PSP groups than in the OA group. These data prove that the PSP plays a more substantial role in inhibiting the catabolic process than the anabolic process, which is sufficient for the reconstruction of inflamed cartilage in OA therapy.

2.6.2. The superior OA therapeutic effect of the tailored cartilage-armor to previous biomaterials. The pursuit of reconstructing joint lubrication in recent years has been categorized into three primary objectives: natural biolubricants, bio-inspired biolubricants and alternative biolubricants, all of which have been applied to treat OA.[2] Most achievements have not solely prioritized achieving optimal lubrication performance but also harnessed the therapeutic effect from anti-inflammation drugs such as diclofenac sodium[12,44] and celecoxib,[46] as well as HA which has therapeutical potential in anti-inflammation.[11,47] However, the potential deleterious effects associated with the frequent local administration of drugs pose nonnegligible threats. The cartilage surface, characterized by its unique compositions and structures, inherently serves as an ideal lubricating surface. Notably, lubricin has gained prominence for its pivotal role in joint lubrication and prevention of OA. The distinctive properties of lubricin emanate from its specialized structures: a brush-like domain that absorbs and retains water, and a cartilage-binding domain that

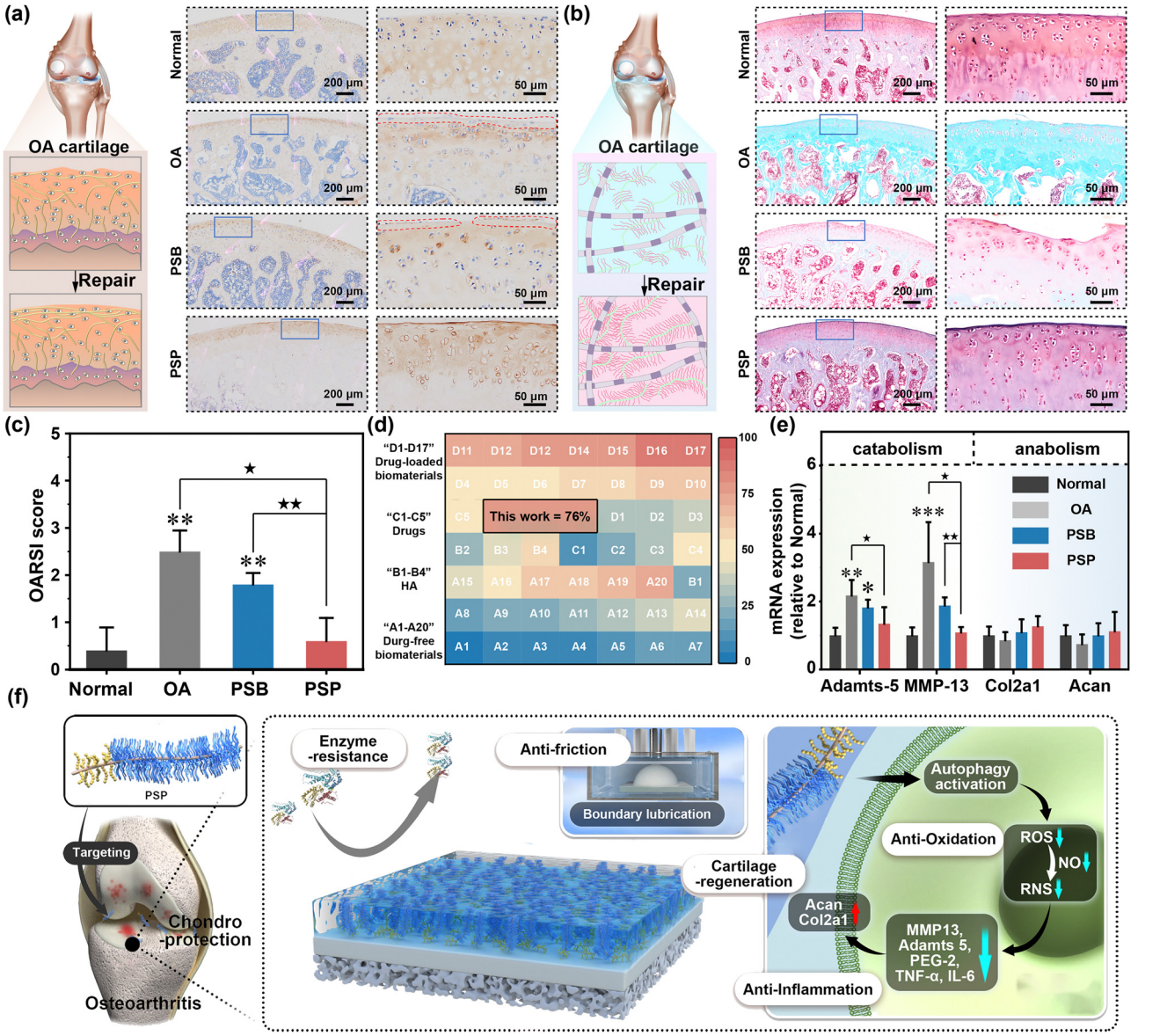

Fig. 7 The therapeutic effect of tailored cartilage armor. (a) The immunohistochemical staining images of Col II, (b) the safranin O-fast green staining images and (c) OARSI scores of normal, OA, PSB and PSP groups. (d) The therapeutic of tailored cartilage armor compared with previous works, in which the absolute values are listed in Table S3 (ESI†) in detail. (e) The relative expression of catabolic genes (Adamts-5 and MMP-13) and anabolic genes (Col2a1 and Acan). (f) Schematic illustration of the chondroprotective properties of tailored cartilage–armor, which are supported by both physicochemical and biological mechanisms. *($p < 0.05$), **($p < 0.01$) and ***($p < 0.001$) are regarded as significant differences in comparison to the normal group. ★($p < 0.05$) and ★★($p < 0.01$) indicated statistical differences between other groups.

adheres to the cartilage matrix.[18] Recognizing the significant impact of lubricin, the development of a lubricin-inspired biomaterials emerges as a promising avenue for OA therapy, particularly with an emphasis on developing materials that can therapeutically intervene in OA without the inclusion of additional drugs. This approach holds promise as a superior and potentially more sustainable strategy for future interventions in OA treatment.

The designed cartilage-armor, strategically engineered to mimic the structure–function relationship inherent in lubricin found in cartilage, specifically encompasses a brush-like lubrication moiety and a binding moiety. PSP was prepared by synthesizing an active ester-containing zwitterion (PSN) and conjugating it with ColBP under weak basic conditions, respectively. The therapeutic effect of cartilage-targeting drug-free PSP stems from a comprehensive interplay of physicochemical and biological mechanisms (Fig. 7f). Following I.A. injection, PSP autonomously homes in on Col II in damaged cartilage. This targeted localization facilitates the formation of an *in situ* hydration layer on the cartilage surface, significantly extending the retention time of PSP in the joint cavity. This property, akin to boundary lubrication, mirrors the physiological functions of lubricin. Additionally, PSP exhibits enhanced ROS/RNS scavenging capabilities, attributable to enzyme-like activities and the

activation of autophagy, surpassing the efficacy of pristine PSB. The establishment of the *in situ* hydration layer by PSP repels catabolic enzymes, thereby providing a pronounced anti-degradation effect. Therefore, PSP restores joint homeostasis by concurrently suppressing catabolic activities and maintaining normal chondrogenic performance. This innovative cartilage-targeting zwitterionic polymer thus holds substantial promise as a therapeutic intervention for conditions characterized by inflammation and friction-related pathologies. The envisaged applications of such polymers extend to a broader spectrum of diseases with analogous etiologies.

2.6.3. The biosafety of the tailored cartilage-armor. A comprehensive blood routine examination is conducted. Analysis of sixteen factors, including granulocyte, white blood cell count, and lymphocyte count, reveals no difference among various groups (normal, OA, PSB and PSP) (Table S2, ESI†). These findings indicate that neither the establishment of the OA model nor the treatment with PSP induces conditions resembling septic arthritis and rheumatoid arthritis during the course of the study. Besides, H&E staining of major organs (heart, liver, spleen, lung and kidney) is performed. The results confirm the absence of any observable damage to thesis vital organs following local treatment with PSP (Fig. S52, ESI†). This collective evidence underscores the favorable systematic biosafety profile of PSP, affirming its suitability for targeted OA therapy without imposing undue threats to systemic health.

3. Conclusions

Biolubrication and sufficient chondrogenesis are crucial for protecting cartilage in the inflammation microenvironment, thereby reconstructing the structures and functions of inflamed cartilage. In this study, we proposed an armor approach to integrating the offensive–defensive process of OA therapy, which is realized using a lubricin-inspired diblock copolymer (PSP). Benefitting from the cartilage-targeting capacity, the tailored cartilage-armor endows durable lubricity and catabolic enzyme-resistance. The enzymatic activities and autophagy activation of the tailored cartilage-armor could effectively scavenge free radicals, thereby promoting chondrogenesis under inflammatory conditions. Thus, this armor approach could exhibit a similar therapeutic effect to most drug-loaded systems in the context of OA. This work not only proposed a lubricin-inspired polymer for targeted therapy of OA, but also implied that activation of autophagy is important for improving hypoxic conditions, thereby suppressing the pathological process of OA.

Author contributions

Peng Yu: conceptualization, investigation, software and writing – original draft. Xu Peng: investigation and resources. Hui Sun, investigation, methodology and formal analysis. Qiangwei Xin: investigation and visualization. Han Kang: software and resources. Peng Wang: investigation and software. Yao Zhao: investigation and formal analysis. Xinyuan Xu: data curation and funding acquisition. Jing Xie: conceptualization, supervision, funding acquisition, writing – review & editing and data curation. Jianshu Li: supervision, funding acquisition, writing – review & editing and project administration.

Data availability

The authors confirm that the data supporting the findings of this study are available within the article and its ESI.†

Conflicts of interest

There are no conflicts to declare.

Acknowledgements

This work was financially supported by the National Natural Science Foundation of China (No. 51925304, 52073191, U22A20158 and 52203180) and the State Key Laboratory of Polymer Materials Engineering (Grant No. sklpme 2023-2-16). The authors are grateful to Life Science Core Facilities (College of Life Sciences, Sichuan University) for the kind help with histological analysis.

References

1 T. Hodgkinson, D. C. Kelly, C. M. Curtin and F. J. O'Brien, *Nat. Rev. Rheumatol.*, 2022, **18**, 67–84.
2 H. Yuan, L. L. E. Mears, Y. Wang, R. Su, W. Qi, Z. He and M. Valtiner, *Adv. Colloid Interface Sci.*, 2022, **311**, 102814.
3 C. Y. Lin, Y. L. Wang, Y. J. Chen, C. T. Ho, Y. H. Chi, L. Y. Chan, G. W. Chen, H. C. Hsu, D. W. Hwang, H. C. Wu and S. C. Hung, *Nat. Biomed. Eng.*, 2022, **6**, 1105–1117.
4 W. Lin and J. Klein, *Adv. Mater.*, 2021, **33**, 2005513.
5 L. Ma, A. Gaisinskaya–Kipnis, N. Kampf and J. Klein, *Nat. Commun.*, 2015, **6**, 6060.
6 Y. Zhang, S. Li, P. Jin, T. Shang, R. Sun, L. Lu, K. Guo, J. Liu, Y. Tong, J. Wang, S. Liu, C. Wang, Y. Kang, W. Zhu, Q. Wang, X. Zhang, F. Yin, Y. E. Sun and L. Cui, *Nat. Commun.*, 2022, **13**, 2447.
7 D. Li, C. Wang, Z. Li, H. Wang, J. He, J. Zhu, Y. Zhang, C. Shen, F. Xiao, Y. Gao, X. Zhang, Y. Li, P. Wang, J. Peng, G. Cai, B. Zuo, Y. Yang, Y. Shen, W. Song, X. Zhang, L. Shen and X. Chen, *Cell Death Dis.*, 2018, **9**, 840.
8 P. Yu, Y. Li, H. Sun, H. Zhang, H. Kang, P. Wang, Q. Xin, C. Ding, J. Xie and J. Li, *Adv. Mater.*, 2023, **35**, 2303299.
9 Z. Peng, H. Sun, V. Bunpetch, Y. Koh, Y. Wen, D. Wu and H. Ouyang, *Biomaterials*, 2021, **268**, 120555.
10 Q. Li, C. Wen, J. Yang, X. Zhou, Y. Zhu, J. Zheng, G. Cheng, J. Bai, T. Xu, J. Ji, S. Jiang, L. Zhang and P. Zhang, *Chem. Rev.*, 2022, **122**, 17073–17154.
11 R. Xie, H. Yao, A. S. Mao, Y. Zhu, D. Qi, Y. Jia, M. Gao, Y. Chen, L. Wang, D. A. Wang, K. Wang, S. Liu, L. Ren and C. Mao, *Nat. Biomed. Eng.*, 2021, **5**, 1189–1201.
12 W. Qiu, W. Zhao, L. Zhang, H. Wang, N. Li, K. Chen, H. Zhang and Y. Wang, *Adv. Funct. Mater.*, 2022, **32**, 2208189.

13 L. Yang, H. Huang, H. Zeng, X. Zhao, R. Wang, Z. Ma, Z. Fan, Y.-M. Liang, S. Ma and F. Zhou, *Carbohydr. Polym.*, 2023, **304**, 120503.
14 P. Yu, Y. Li, H. Sun, X. Ke, J. Xing, Y. Zhao, X. Xu, M. Qin, J. Xie and J. Li, *ACS Appl. Mater. Interfaces*, 2022, **14**, 27360–27370.
15 Y. Lei, Y. Wang, J. Shen, Z. Cai, Y. Zeng, P. Zhao, J. Liao, C. Lian, N. Hu, X. Luo, W. Cui and W. Huang, *Adv. Funct. Mater.*, 2021, **31**, 2105084.
16 P. Xiao, X. Han, Y. Huang, J. Yang, L. Chen, Z. Cai, N. Hu, W. Cui and W. Huang, *Bioact. Mater.*, 2024, **32**, 242–259.
17 M. Wu, K. Zheng, W. Li, W. He, C. Qian, Z. Lin, H. Xiao, H. Yang, Y. Xu, M. Wei, J. Bai and D. Geng, *Adv. Funct. Mater.*, 2023, **34**, 2305603.
18 Z. Sun, E. Feeney, Y. Guan, S. G. Cook, D. Gourdon, L. J. Bonassar and D. Putnam, *Proc. Natl. Acad. Sci. U. S. A.*, 2019, **116**, 12437–12441.
19 G. W. Greene, X. Banquy, D. W. Lee, D. D. Lowrey, J. Yu and J. N. Israelachvili, *Proc. Natl. Acad. Sci. U. S. A.*, 2011, **108**, 5255–5259.
20 X. Banquy, J. Burdyńska, D. W. Lee, K. Matyjaszewski and J. Israelachvili, *J. Am. Chem. Soc.*, 2014, **136**, 6199–6202.
21 G. Morgese, E. Cavalli, M. Muller, M. Zenobi–Wong and E. M. Benetti, *ACS Nano*, 2017, **11**, 2794–2804.
22 A. Singh, M. Corvelli, S. A. Unterman, K. A. Wepasnick, P. McDonnell and J. H. Elisseeff, *Nat. Mater.*, 2014, **13**, 988–995.
23 H. J. Faust, S. D. Sommerfeld, S. Rathod, A. Rittenbach, S. Ray Banerjee, B. M. W. Tsui, M. Pomper, M. L. Amzel, A. Singh and J. H. Elisseeff, *Biomaterials*, 2018, **183**, 93–101.
24 Y. Zhao, X. Deng, S. Tan, J. Zhang, J. Han, X. Wang, J. Pei, H. Li, X. Deng, C. Yin, D. Yin, Y. Tian and A. Qian, *Adv. Healthcare Mater.*, 2022, **12**, 2202143.
25 S. Xue, X. Zhou, W. Sang, C. Wang, H. Lu, Y. Xu, Y. Zhong, L. Zhu, C. He and J. Ma, *Bioact. Mater.*, 2021, **6**, 2372–2389.
26 W. Xiong, Q. Lan, X. Liang, J. Zhao, H. Huang, Y. Zhan, Z. Qin, X. Jiang and L. Zheng, *J. Nanobiotech.*, 2021, **19**, 197.
27 G. V. Ferrari, J. Natera, M. Paulina Montana, V. Munoz, E. L. Gutierrez, W. Massad, S. Miskoski and N. A. Garcia, *J. Photochem. Photobiol., B*, 2015, **153**, 233–239.
28 A. Das and P. Theato, *Chem. Rev.*, 2016, **116**, 1434–1495.
29 G. Morgese, E. Cavalli, J.-G. Rosenboom, M. Zenobi-Wong and E. M. Benetti, *Angew. Chem., Int. Ed.*, 2018, **57**, 1621–1626.
30 A. Vedadghavami, T. He, C. Zhang, S. M. Amiji, B. Hakim and A. G. Bajpayee, *Acta Biomater.*, 2022, **151**, 278–289.
31 P. Yu, Y. Liu, J. Xie and J. Li, *J. Controlled Release*, 2021, **338**, 486–504.
32 R. Zhang, Y. Liu, M. He, Y. Su, X. Zhao, M. Elimelech and Z. Jiang, *Chem. Soc. Rev.*, 2016, **45**, 5888–5924.
33 Z. Yang, Y. He, S. Liao, Y. Ma, X. Tao and Y. Wang, *Sci. Adv.*, 2021, **7**, eabf9117.
34 M. Wathier, B. A. Lakin, B. G. Cooper, P. N. Bansal, A. M. Bendele, V. Entezari, H. Suzuki, B. D. Snyder and M. W. Grinstaff, *Biomaterials*, 2018, **182**, 13–20.
35 R. F. Loeser, J. A. Collins and B. O. Diekman, *Nat. Rev. Rheumatol.*, 2016, **12**, 412–420.
36 Y. Chen, Y. Wang, Z. Chen, J. Cai, K. Li, H. Huang, F. Song, M. Gao, Y. Yang, L. Zheng and J. Zhao, *Mater. Today Nano*, 2022, **19**, 100240.
37 G. Yang, M. Fan, J. Zhu, C. Ling, L. Wu, X. Zhang, M. Zhang, J. Li, Q. Yao, Z. Gu and X. Cai, *Biomaterials*, 2020, **255**, 120155.
38 Y. Shi, X. Hu, J. Cheng, X. Zhang, F. Zhao, W. Shi, B. Ren, H. Yu, P. Yang, Z. Li, Q. Liu, Z. Liu, X. Duan, X. Fu, J. Zhang, J. Wang and Y. Ao, *Nat. Commun.*, 2019, **10**, 1914.
39 Y. Ding, Z. Li, W. Hu, X. Feng, Y. Chen, G. Yan, Y. Wang, B. Zhu, W. Yao, L. Zheng, M. He, M. Gao and J. Zhao, *Biomater. Sci.*, 2021, **9**, 6236–6250.
40 P. Vega–Vasquez, N. S. Mosier and J. Irudayaraj, *ACS Nano*, 2021, **15**, 8338–8349.
41 L. Fu, P. Li, J. Wu, Y. Zheng, C. Ning, Z. Liao, X. Yuan, Z. Ding, Z. Zhang, X. Sui, S. Shi, S. Liu and Q. Guo, *Regen. Biomater.*, 2023, **10**, rbad085.
42 L. He, Y. Pan, J. Yu, B. Wang, G. Dai and X. Ying, *Int. Immunopharmacol.*, 2021, **97**, 107657.
43 Y. Yan, T. Sun, H. Zhang, X. Ji, Y. Sun, X. Zhao, L. Deng, J. Qi, W. Cui, H. A. Santos and H. Zhang, *Adv. Funct. Mater.*, 2019, **29**, 1807559.
44 L. Yang, L. Sun, H. Zhang, F. Bian and Y. Zhao, *ACS Nano*, 2021, **15**, 20600–20606.
45 Y. Lei, Y. Wang, J. Shen, Z. Cai, C. Zhao, H. Chen, X. Luo, N. Hu, W. Cui and W. Huang, *Sci. Adv.*, 2022, **8**, eabl6449.
46 Y. Lei, X. Wang, J. Liao, J. Shen, Y. Li, Z. Cai, N. Hu, X. Luo, W. Cui and W. Huang, *Bioact. Mater.*, 2022, **16**, 472–484.
47 L. J. Kang, J. Yoon, J. G. Rho, H. S. Han, S. Lee, Y. S. Oh, H. Kim, E. Kim, S. J. Kim, Y. T. Lim, J. H. Park, W. K. Song, S. Yang and W. Kim, *Biomaterials*, 2021, **275**, 120967.